Available online at www.sciencedirect.com
SCIENCE DIRECT®
ELSEVIER
European Journal of Mechanics B/Fluids 22 (2003) 379–390

Flow structures in zero pressure-gradient turbulent boundary layers at high Reynolds numbers

Jens M. Österlund *,[1], Björn Lindgren, Arne V. Johansson

Department of Mechanics, KTH, SE-100 44 Stockholm, Sweden

Received 22 March 2000; received in revised form 10 February 2003; accepted 10 April 2003

Abstract

The near-wall region of zero-pressure gradient turbulent boundary layers was studied through correlation- and other two-point measurements over a wide range of Reynolds numbers. The requirements of high spatial resolution were met by use of a MEMS-type of hot-film sensor array together with a small, in-house built hot-wire probe. Streak-spacing and characteristics of buffer region shear-layer events were studied. At high Reynolds numbers the motions that are of substantially larger scale than the streaks have a significant influence on the near-wall dynamics. By removing such scales through high-pass filtering a streak spacing was recovered that is close to that found in low Reynolds number flows. The frequency of occurrence of shear-layer events was found to scale with a mixed time scale, in analogy with earlier findings in channel flow, again indicating the increasing relative influence of large scales with increasing Reynolds number.

1. Introduction

The statistical, Reynolds averaged, description of turbulent boundary layers hides a wealth of structure-related phenomena with, e.g., a quite intermittent character of the turbulence production. This has been illustrated in flow visualizations, measurements and from DNS-generated data in a large number of papers, see, e.g., the landmark paper of Kline et al. [1], who showed that a significant part of the turbulence could be described in terms of deterministic events. These studies showed that in the close proximity of the wall the flow is characterized by elongated regions of low and high speed fluid of fairly regular spanwise spacing of about $\lambda^+ = 100$. Sequences of ordered motion occur randomly in space and time where the low-speed streaks begin to oscillate and to suddenly break-up into a violent motion, a "burst". Kim et al. [2] found the intermittent bursting process to be closely related to shear-layer like flow structures in the buffer region, and also roughly 70% of the total turbulence production to be associated with the bursting process. The "bursts" were further investigated by Corino and Brodkey [3] who divided the turbulence producing events into two kinds. The ejection: involving rapid outflow of low speed fluid from the wall and sweeps: large scale motions originating in the outer region approaching the wall. Smith and Metzler [4] investigated the characteristics of low-speed streaks using hydrogen bubble-flow and a high-speed video system. They found that the streak spacing increases with the distance from the wall. Furthermore, they found the persistence of the streaks to be one order of magnitude larger than the observed bursting times associated with the near-wall region turbulence producing events.

Many different schemes have been proposed for the structure identification, using one or more components of the velocity or the wall-shear stress. The qualitative and quantitative features of the structures are then normally found through conditional averaging of the detected events as was first employed by Kovasznay et al. [5]. One should keep in mind, though, the unavoidable

* Corresponding author.
E-mail address: odj@foi.se (J.M. Österlund).
[1] Presently at the Swedish Defence Research Agency, Aeronautics, SE–172 90 Stockholm, Sweden.

0997-7546/$ – see front matter
doi:10.1016/S0997-7546(03)00034-7

subjectivity inferred by the choice of detection. A comprehensive comparison between different schemes and the kind of events they identify can be found in Yuan and Mokhtarzadeh-Dehghan [6]. Wallace et al. [7] and Willmarth and Lu [8] introduced the uv quadrant splitting scheme. Blackwelder and Kaplan [9] developed the VITA technique to form a localized measure of the turbulent kinetic energy and used it to detect shear-layer events. The detected events were studied using conditional averaging. Chen and Blackwelder [10] added a slope condition to the VITA technique to detect only events corresponding to rapid acceleration. The behavior of the conditionally averaged streamwise velocity detected on strong accelerating events may be explained by tilted shear-layers that are convected past the sensor. Tardu [11] introduced a detection method that differ between single and multiple shear-layer events and found that the contribution to the Reynolds shear-stress is larger from the latter. Kreplin and Eckelmann [12] measured the angle of the shear-layer front from the wall and found that it was about 5° in the immediate vicinity of the wall. In the buffer region the inclination angle of the shear layer has been found to be about 15–20°. This angle is much smaller than that of typical outer-layer flow structures. Head and Bandyopadhyay [13] found that angle to be about 45°.

Gupta et al. [14] investigated the spatial structure in the viscous sub-layer using an array of hot-wires distributed in the spanwise direction. They used a VITA correlation technique to determine the spanwise separations between streaks in the viscous-sub layer. The evolution of shear layers was studied by Johansson et al. [15] in the Göttingen oil channel by use of two-probe measurements in the buffer region of the turbulent channel flow. Wark and Nagib [16] studied coherent structures in turbulent boundary layers at moderate Reynolds number using a quadrant detection technique. They found that a large part of the events are relatively large in scale. They also found that there is a hierarchy of sizes and that the outer flow influences the bursting process. The bursting frequency in turbulent boundary layers was first investigated by Rao et al. [17], their experiments indicated that outer scaling gave the best collapse of the data. Later, Blackwelder and Haritonidis [18] carried out experiments on the bursting frequency in turbulent boundary layers. They found the non-dimensional bursting frequency was independent of Reynolds number when scaled with the inner time scale and found a strong effect of spatial averaging for sensors larger than 20 viscous length scales. Alfredsson and Johansson [19] studied the frequency of occurrence for bursts in turbulent channel flow, where they found the governing time scale to be a mixture (the geometric mean) of the inner and outer time scales. Johansson et al. [20] analyzed near-wall flow structures obtained from direct numerical simulation of channel flow Kim et al. [35] using conditional sampling techniques. They also analyzed the space–time evolution of structures and asymmetry in the spanwise direction was found to be an important characteristic of near-wall structures, and for shear-layers in particular.

There seems to be no consensus on how to define a coherent structure and several definitions exist. In a review article on the subject Robinson [21] defines a coherent structure as

> ...a three-dimensional region of the flow over which at least one fundamental flow variable (velocity component, density, temperature, etc.) exhibits significant correlation with itself or with another variable over a range of space and/or time that is significantly larger than the smallest local scales of the flow.

Other more restricted definitions are given by, e.g., Hussain [22] and Fiedler [23]. Here we will deal mainly with the streaks found in the viscous sub-layer and the connected shear-layer type structures that are believed to be important contributors to the turbulence generation.

The majority of the experimental studies on structures in zero pressure gradient turbulent boundary layers have been conducted at low Reynolds numbers ($Re_\theta < 5000$), where flow visualization and high resolution velocity measurements are relatively easy to obtain. One of the objectives with this study was therefore to extend the knowledge about turbulence structures to high Reynolds numbers, in particular the issue of the relative importance on outer scale motions on the near-wall dynamics.

Three types of investigations were carried out. First, we investigate the mean streak spacing by measurements of the instantaneous wall-shear stress in two points with different spanwise separations. Secondly, the scaling of the "bursting frequency" was investigated by detection of the frequency of VITA events in the buffer region. Thirdly, a single wire probe was traversed in a streamwise wall-normal (x, y)-plane above the hot-film sensor, with the aim to detect and characterize shear-layer type events and to determine their spatial structure and local propagation velocity.

2. Experimental facility

The flow field of a zero pressure-gradient turbulent boundary layer was established on a 7 meter long flat plate mounted in the test section of the MTL wind-tunnel at KTH. The MTL wind tunnel is of closed-return type designed with low disturbance level as the primary design goal.

The flow quality of the MTL wind-tunnel was reported by Johansson [24]. For instance, the streamwise turbulence intensity was found to be less than 0.02%. The air temperature can be controlled to within $\pm 0.05\,^\circ$C, which is very important for this study since the primary measurement technique was hot-wire/hot-film anemometry, where a constant air temperature during

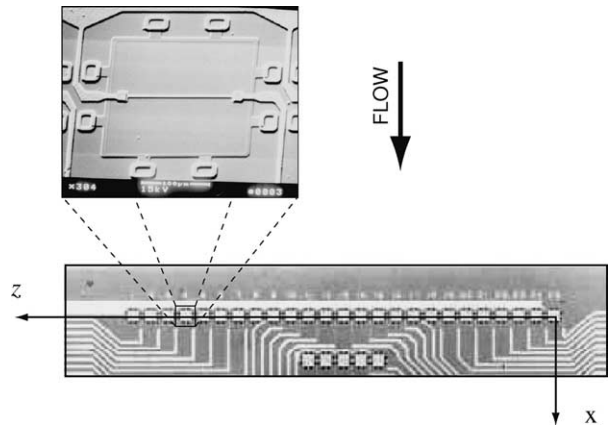

Fig. 1. Enlargement of the MEMS hot-film wall-shear stress sensor chip from UCLA/Caltech [25] showing the array of 25 sensors used, seen as the row of white squares on the z-axis. A blow-up of one of the hot-films is also shown.

the measurement is a key issue. The test section has a cross sectional area of 0.8 m × 1.2 m (height × width) and is 7 m long. The upper and lower walls of the test section can be moved to adjust the pressure distribution. The maximum variation in mean velocity distribution along the boundary layer plate was ±0.15%.

The first 5.5 m of the plate was used for the experiment. One of the plate sections was equipped with two circular inserts, one for a plexiglas plug where the measurements were done, and one for the traversing system. The traversing system was fixed to the plate to minimize any vibrations and possible deflections. The distance to the wall from the probe was determined by a high magnification microscope. The absolute error in the determination of the wall distance was within ±5 μm.

The boundary layer was tripped using several rows of tape with raised V-shapes at the beginning of the plate and the two-dimensionality of the boundary layer was checked by measuring the spanwise variation of the wall shear stress τ_w. The maximum spanwise variation in friction velocity $u_\tau = \sqrt{\tau_w/\rho}$ was found to be less than ±0.7%.

The reference conditions used in the calibration of the probes were determined using a Prandtl tube in the free-stream directly above the measurement station. The accuracy of the pressure measurement was 0.25% and the accuracy of the temperature measurement was 0.02°C.

Constant temperature hot-wire anemometry was used in all velocity measurements. All hot-wire probes were designed and built at the lab. Three sizes of single-wire probes were used in the experiments with wire diameters of: 2.5, 1.27 and 0.63 μm and a length to diameter ratio always larger than 200.

The MEMS hot-film (Fig. 1) used in the wall-shear stress measurements was designed by the MEMS group at UCLA/Caltech [25–27]. It was flush-mounted with a printed circuit board for electrical connections which in turn was flush-mounted into a Plexiglas plug fitting into the instrumentation insert of the measurement plate-section. The MEMS sensor chip has four rows of 25 sensors with a spanwise separation of 300 μm, see Fig. 1. The length of each hot-film is 150 μm and the width 3 μm. It is placed on a 1.2 μm thick silicon–nitrite diaphragm with dimensions 200 μm × 200 μm. Thermal insulation of the hot-film to the substrate is provided by a 2 μm deep vacuum cavity underneath the diaphragm.

The anemometer system (AN1003 from AA lab systems, Israel) has a built-in signal conditioner and the signals from the anemometer were digitized using an A/D converter board (A2000 from National Instruments, USA) in the measurement computer. The A/D converter has 12 bit resolution and four channels which could be sampled simultaneously at rates up to 1 MHz divided by the number of channels used.

3. Experimental procedure

3.1. Probe calibration

The hot-wires were calibrated in the free-stream against the velocity obtained from a Prandtl tube at 10 different speeds ranging from about 5% to 100% of the free-stream velocity of the actual experiment. A least-squares fit of the anemometer voltage versus the velocity was formed using King's law.

The hot-films were calibrated *in situ* in the turbulent boundary layer against the mean skin-friction obtained from oil-film interferometry, here denoted τ_w^*.

The principle of oil-film interferometry is to register the temporal deformation of a thin film of oil, due to the shear stress, from the flow, on its upper surface. From the deformation velocity the wall-shear stress can be determined accurately, knowing the viscosity of the oil. The oil-film deformation velocity was determined by measuring the thickness of the oil-film by interferometry, see Fernholz et al. [28]. A least-squares fit of a variant of the logarithmic skin-friction law of the type

$$c_f = 2\left[\frac{1}{\kappa}\ln(Re_\theta) + C\right]^{-2} \tag{1}$$

was made to the obtained wall-shear stress, with the resulting values of the constants $\kappa = 0.384$ and $C = 4.08$, see Fig. 2. Comparisons with other methods and also other experiments are made in Österlund et al. [29].

After the mean wall-shear stress relation was determined the anemometer voltage signals, from the two wall-shear stress sensors to be calibrated, were recorded for eight different mean wall-shear stress values in the range $0.3 < \tau_w^* < 3$ times the mean value of interest. This large range was necessary, due to the long tails of the probability density function for τ_w, to avoid extrapolation of the calibration function (2). Kings law was used to relate the anemometer output voltage E to the instantaneous skin-friction τ_w,

$$\tau_w = \left[\frac{1}{B}\left(E^2 - A\right)\right]^{1/n}, \tag{2}$$

where A, B and n are constants. The constants in Eq. (2) were determined minimizing the sum of the mean-square-error, for all calibration points, between the measured mean skin-friction, τ_w^*, and the mean value, $\overline{\tau_w}$, obtained applying relation (2) to the anemometer voltage signal E:

$$\min\left(\sum(\tau_w^* - \overline{\tau_w})^2\right). \tag{3}$$

The dynamical range of the MEMS hot-film probe allowed for measurements in the Reynolds number range $7500 < Re_\theta < 12500$. The MEMS hot-film was found to give a relative fluctuation intensity of 0.35 (at $Re_\theta \approx 12400$), i.e., somewhat lower than the commonly reported value of 0.41, see Österlund [30]. This deviation reflects a limitation of the sensor technique but should not be of significant influence for the present correlation measurements.

3.2. Mean flow characteristics

Velocity profiles at five different streamwise positions ($x = 1.5, 2.5, \ldots, 5.5$ m) were taken over a large span in Reynolds number ($2530 < Re_\theta < 27300$), see Fig. 2. The behavior of the boundary layer was found to confirm the traditional two layer theory with a logarithmic overlap region for $200\nu/u_\tau < y < 0.15\delta_{95}$ existing for $Re_\theta > 6000$. δ_{95} is the boundary layer thickness where the mean streamwise velocity is 95% of the free-stream velocity. It is here used instead of the more common δ_{99} because it can be determined experimentally much more accurately. This difference does not affect the scaling of the boundary layer, see Österlund [30]. The values of the von Kármán constant and the additive constants were found to be $\kappa = 0.38$, $B = 4.1$ and $B_1 = 3.6$, see Österlund et al. [29]. (This slightly lower value of the von Kármán constant than the standard value of 0.4 has also been found by others, see, e.g., the reevaluation of the superpipe data by Perry et al. [32]).

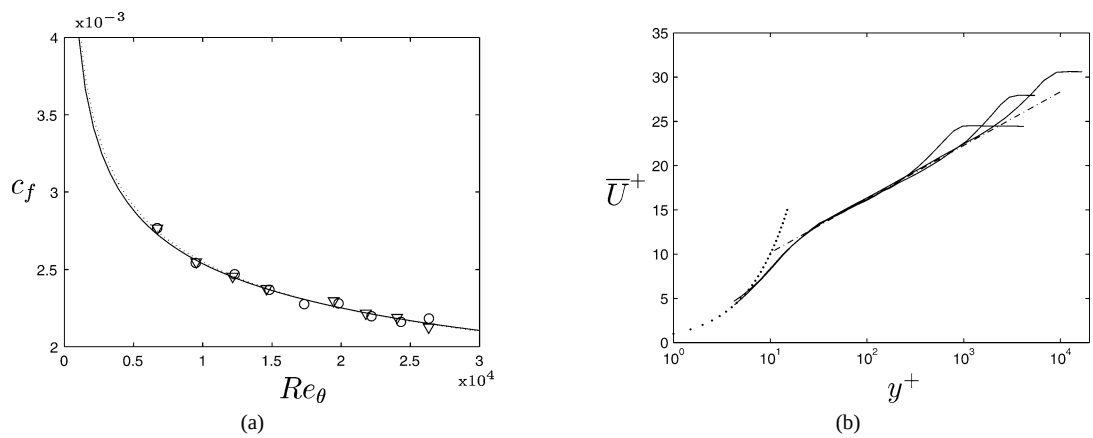

Fig. 2. Mean flow characteristics of the boundary layer. $2530 < Re_\theta < 27300$. (a) Skin-friction coefficient. ∘ and ▽: oil-film interferometry. –·–: best-fit of logarithmic friction law (equation (1)) to the oil-film data. —: Skin-friction law from Fernholz and Finley [31]. (b) Mean velocity profiles for $Re_\theta = 2530$, 9700 and 27300. Dotted and dashed curves represent $U^+ = y^+$ and $U^+ = \frac{1}{0.38}\ln y^+ + 4.1$.

3.3. Detection of events

In the detection of shear layer structures the variable-interval time average (VITA) was used. The VITA of a fluctuating quantity $Q(x_i, t)$ is defined by

$$\widehat{Q}(x_i, t, T) = \frac{1}{T} \int_{t-T/2}^{t+T/2} Q(s)\,\mathrm{d}s, \tag{4}$$

where T is the averaging time. The conventional time average results when T becomes large, i.e.,

$$\overline{Q}(x_i) = \lim_{T\to\infty} \widehat{Q}(x_i, t, T). \tag{5}$$

Blackwelderand Kaplan [9] used the VITA technique to form a localized measure of the turbulent energy

$$var(x_i, t, T) = \frac{1}{T} \int_{t-T/2}^{t+T/2} u^2(s)\,\mathrm{d}s - \left(\frac{1}{T} \int_{t-T/2}^{t+T/2} u(s)\,\mathrm{d}s\right)^2. \tag{6}$$

This quantity is also known as the short-time variance of the signal. The VITA variance can be used to detect shear-layer type events. An event is considered to occur when the amplitude of the VITA variance exceeds a certain threshold level. A detection function is defined as

$$D_u(t, T) = \begin{cases} 1 & var > k\overline{u^2} \text{ and } \frac{\partial u}{\partial t} > 0, \\ 0 & \text{otherwise}, \end{cases} \tag{7}$$

where k is the detection threshold level. The correspondence between shear-layers and VITA events was substantiated by, e.g., Johansson and Alfredsson [33] and Johansson et al. [34].

A set of events $E_u = \{t_1, t_2, \ldots, t_N\}$ was formed from the midpoints of the peaks in the detection function D_u. Conditional averages of a quantity Q can then be constructed as

$$\langle Q(\tau)\rangle = \frac{1}{N} \sum_{j=1}^{N} Q(t_j + \tau), \tag{8}$$

where τ is the time relative to the detection time and N is the total number of detected events.

In addition to detecting events using the VITA variance technique, events were detected on the amplitude of the fluctuating quantity itself, e.g., detection of peaks of the fluctuating wall-shear stress,

$$D_{\tau_w}(t, T) = \begin{cases} 1 & \tau_w > k\sqrt{\overline{\tau_w^2}}, \\ 0 & \text{otherwise}. \end{cases} \tag{9}$$

4. Results

4.1. Streak spacing

The mean spanwise separation between low-speed streaks in the viscous sub-layer was investigated using the MEMS array of hot-films, see Fig. 1. It gave us 18 spanwise separations in the range $0 \leqslant \Delta z^+ \leqslant 210$. The spanwise length of the hot-films was $l^+ = 5.6$, at the Reynolds number $Re_\theta = 9500$ ($Re_\tau \equiv \delta_{95} u_\tau/\nu = 2300$). The spanwise cross correlation coefficient between the wall-shear stress signals obtained from two hot-films separated a distance Δz^+ in the spanwise direction is defined by

$$R_{\tau_w\tau_w}(\Delta z) = \frac{\overline{\tau_w(z)\tau_w(z+\Delta z)}}{\tau_w'^2}, \tag{10}$$

where prime denotes r.m.s. value. The cross-correlation coefficient was used to estimate the mean streak spacing.

At low Reynolds numbers the low-speed streaks, and their associated lift-up and ejection outwards, represent a dominant feature in the near-wall turbulence. An interesting issue is to what extent this also holds as the Reynolds number is increased. The answer to this question should give an important indication about the relative importance of outer scale motions for near-wall dynamics. For instance, we will later return to the issue of the scaling of the frequency of occurrence of buffer region shear-layer structures.

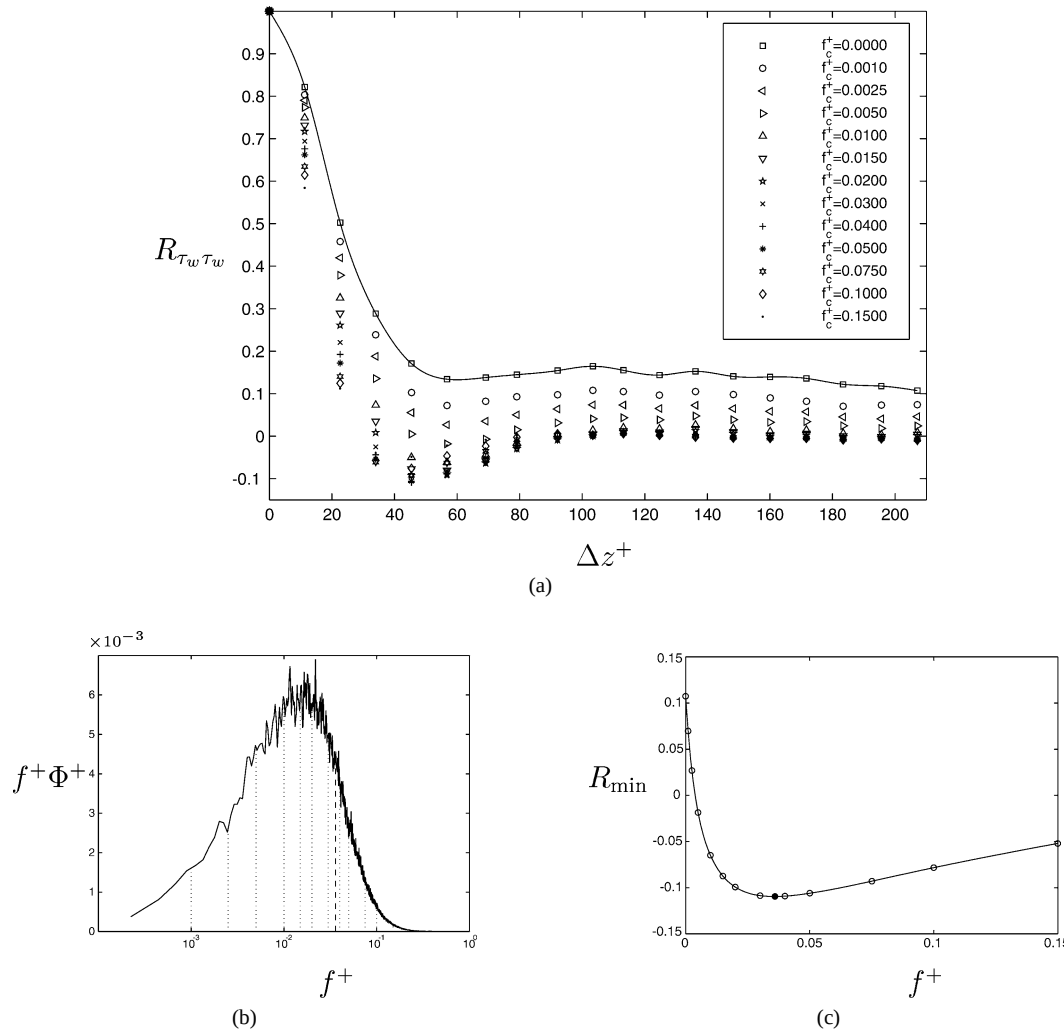

Fig. 3. Determination of the optimum high-pass filter at $Re_\theta = 9500$. (a) Two-point correlation function $R_{\tau_w\tau_w}(\Delta z^+)$ for various degrees of high-pass filtering, (cut-off frequencies given in diagram). The solid line is a spline fit to the unfiltered case. (b) Spectrum from wall shear-stress measurement. Vertical dotted lines indicates the high-pass filter cut-off frequencies in diagram a. Dashed vertical line is the cut-off frequency that minimizes the correlation function, $f_c^+ = 0.036$. (c) Minimum values of the correlation function for varying cut-off frequency (○). Solid line: spline fit to data. ●: Absolute minimum found from spline.

At low Reynolds numbers the dominance of the streaks in the viscous sublayer gives a distinct negative minimum in the spanwise correlation function for a spanwise separation of about 50 viscous length units. This is in accordance with the, from flow visualizations, observed mean streak spacing of about $100\nu/u_\tau$. In Fig. 3(a) the correlation function $R_{\tau_w\tau_w}(\Delta z^+)$ is shown for a momentum loss Reynolds number of 9500, and we can observe that no clear minimum is visible without filtering of the time signal. This indicates that, at this relatively high Reynolds number outer scale motions and dynamics become of importance even in the immediate vicinity of the wall. Similar observations have also been found by others, see, e.g., Gupta et al. [14] and Naguib and Wark [37]. In the later paper the authors filtered the time signal using a band-pass filter with varying frequency to identify the scaling of the correlation function between a wall-wire and a single-wire traversed from the buffer region outwards at Reynolds numbers based on the momentum loss thickness between 1579 and 5961.

A trend is clearly visible in the relatively low Reynolds number simulations by Kim et al. [35] and Moser et al. [36] where at their highest Reynolds number the minimum is less pronounced. One could hypothesize that the pattern of streaky sub-layer structures at high Reynolds numbers still exists but becomes increasingly concealed by contributions from large scale motions, as the range of scales increases. This hypothesis is also supported by a recent "high" Reynolds number ($Re_\tau = 640$ based on half channel height and friction velocity) DNS of channel flow by Abe and Kawamura [38] (complemented with private

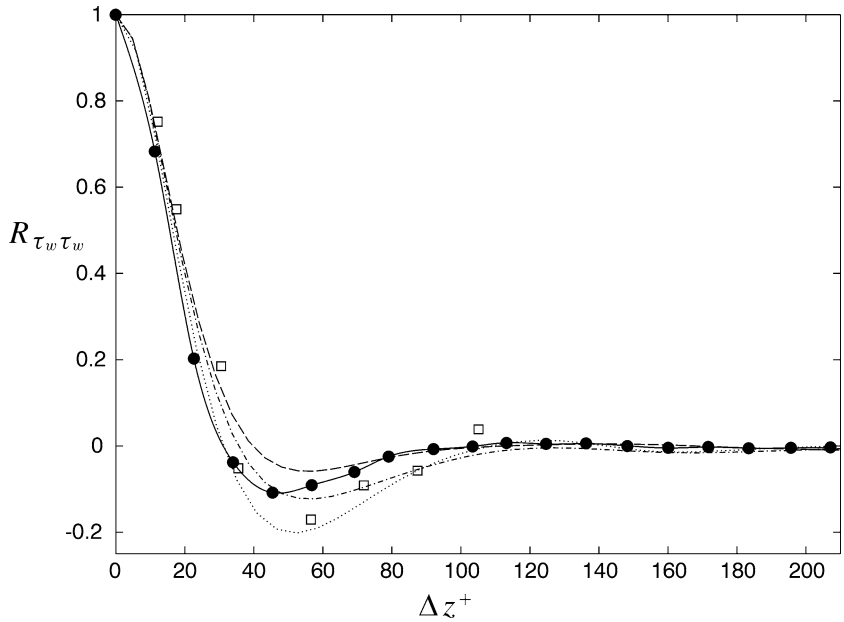

Fig. 4. Streak spacing comparison with other data from experiments and DNS. •: Present data with $f_c^+ = 0.036$, —: spline fit to present data. DNS of channel flow, correlations of u at $y^+ = 5$, − −: $Re_\tau = 590$, − · −: $Re_\tau = 395$, ···: $Re_\tau = 180$ [35,36]. Measurement in channel flow, correlations of u at $y^+ = 5$, □: $Re_\tau = 200$ [12].

communication) which shows a very weak minimum in the $R_{\tau_w\tau_w}(\Delta z^+)$ correlation function. They also reveal these large scale structures near the wall by means of low-pass filtering. In an attempt to reveal and possibly obtain the streak spacing also from the high Reynolds number data in the present experiment we applied a high-pass (Chebyshev phase-preserving) digital filter to the wall-shear stress signals before calculating the correlation coefficient. This procedure emphasizes the contribution from the near-wall streaks and enhances the variation in the correlation coefficient.

With increasing cut-off frequency the minimum in the correlation function first becomes more pronounced but at very large cut-off frequencies the minimum tends to disappear again (see Fig. 3(a)). An investigation was performed to find the cut-off frequency that gives the most pronounced minimum in the correlation function. Since the streaks are responsible for the negative correlation values the optimum filtering cut-off should be high enough to remove the influence from larger flow structures. In Fig. 3(c) the minimum value of the correlation function is plotted against the cut-off frequency. The filled circle indicates the minimum and the value of the cut-off frequency here was found to be 0.036 in inner scaling. A calculation of the correlation function was performed with this particular cut-off frequency. The result is shown as filled circles in Fig. 4. It is interesting to notice that the minimum cut-off frequency of 0.036 can be translated to a length scale in inner variables, l^+, of approximately 400. This is close to the expected mean length of a streak.

The broad minimum in Fig. 3(c) is consistent with the fact that the streaks vary significantly in size. Note that also band-pass filtering was tested to remove influence of high frequency contributions to the correlation function but no significant effect could be found above that from the high-pass filtering. An explanation of this is that the energy content above, say $f^+ = 0.1$, is very small, as can be seen in Fig. 3(b). The dotted vertical lines in Fig. 3(b) represent the cut-off frequencies used in Fig. 3(a). The dashed vertical line is the chosen cut-off frequency of 0.036.

When plotted as in Fig. 3(b) the area under the curve directly represents the kinetic energy content. We may notice the large amount of energy located at lower frequencies than the chosen cut-off frequency. This points to the fact that the streaks play a less important role in the near-wall dynamics at high Reynolds number. This fact may also have an impact on control strategies for high Reynolds number flows.

The value of the separation, Δz^+, for which correlation attains a minimum, was found to vary (decrease) only slightly with increasing cut-off frequency. The location of the minimum of the correlation function was at $\Delta z^+ = 48$ for a cut-off frequency of $f_c^+ = 0.036$. This corresponds to a streak spacing of 96, which lies in the range of values from other experiments and direct numerical simulations. The typical value for the streak spacing given is 100.

The filtered correlation function, see Fig. 4, is close to zero for separations $\Delta z^+ > 100$. This result agrees well with other experiments and simulations at low Reynolds numbers, see, e.g., Kline et al. [1], Kreplin and Eckelmann [12], Smith and Metzler [4], Kim et al. [35] and Moser et al. [36], some of which are included in Fig. 4 for comparison Gupta et al. [14] computed two-

point correlations with spanwise separation in the near-wall region. They show results mostly from $Re_\theta = 3300$ where the (unfiltered) correlation function is of similar character to that shown in Fig. 3(a). They noted the lack of a clear minimum in the correlation function, and instead used the VITA technique to extract some information on characteristic spanwise scales.

4.2. Propagation velocities

The space–time correlation of the wall-shear stress and the streamwise velocity was measured using one hot-film sensor and one hot-wire traversed in the (x, y)-plane. The time-shift of the peaks of the correlation coefficient,

$$R_{\tau_w u}(\Delta x, \Delta y, \Delta t) = \frac{\overline{\tau_w(x, y, t)u(x + \Delta x, y + \Delta y, t + \Delta t)}}{\tau'_w u'}, \tag{11}$$

for different Δx and Δy separations are shown in Fig. 5(a). The peak in the correlation moves to negative time-shifts for increasing wall distances, i.e., the structures are seen earlier away from the wall. This indicates a forward leaning structure. The propagation velocity of the structure at different distances from the wall is defined by the slopes

$$C_p^+ = \frac{\Delta x^+}{\Delta t^+} \tag{12}$$

of lines fitted to the time-shifts at constant wall-distance in Fig. 5(a). The resulting propagation velocities are plotted in Fig. 5(b) as filled circles and was found to be approximately constant ($C_p^+ \approx 13$) up to about $y^+ = 30$. Further out it was found to be close to the local mean velocity. This means that the structure becomes stretched by the mean shear above $y^+ = 30$. It can also be seen from the variation of the shear layer angle with wall distance as we will return to later, see Fig. 8. In Fig. 5(b) results from other experiments and simulations are shown as open symbols. The results from channel flow at $Re_\tau \approx 180$ by Johansson et al. [15] are shown in in Fig. 5(b) as squares, and agree well with the present findings. Johansson et al. [20] analyzed DNS data for channel flow at the same Reynolds number with a spatial counterpart to the VITA technique and found the propagation velocity to be 10.6 at $y^+ = 15$. Krogstad et al. [39] investigated the importance of probe separation for the estimation of the propagation velocity. They found a slight variation with increasing measured propagation velocity with increasing separation. The values from their experiment shown in Fig. 5(b) as diamonds are taken at a separation of $\Delta x/\delta$ of 0.1 which corresponds to a value of Δx^+ of about 400. This corresponds well to the range of our least square fit, see Fig. 5(a). Their results are similar to ours although at $y^+ = 38$ it is slightly higher than the expected value of the mean velocity and at $y^+ \leqslant 10$ they found the propagation velocity to be around 11. This value is close to the value found by Johansson et al. [20] although at a smaller y^+.

4.3. Shear-layer events

Shear-layer events were detected from peaks in the short time variance as described in Section 3.3 using the velocity signal from a hot-wire in the buffer layer. In Table 1 an overview is given of the hot-wire measurements used for VITA detection. The detection times are taken as the midpoints of the peaks of the detection function and an ensemble average is formed according to

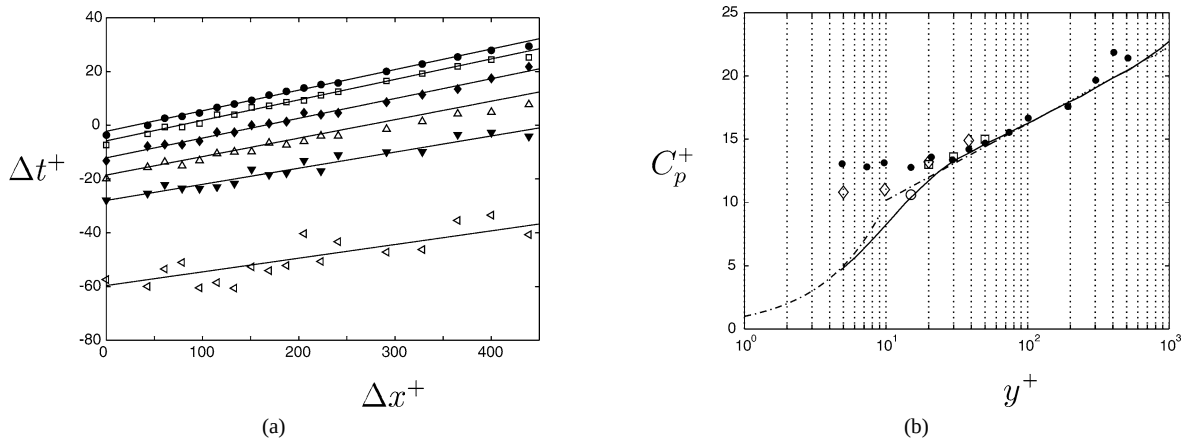

Fig. 5. Propagation velocity in the boundary layer. (a) Time-shift of maximum correlation, $\max(R_{u\tau_w})$. •: $y^+ = 5$. □: $y^+ = 10$. ♦: $y^+ = 20$. △: $y^+ = 50$. ▼: $y^+ = 100$. ◁: $y^+ = 300$. (b) Propagation velocity C_p^+, •: Present data $Re_\theta = 9500$, □: [15] at $Re_\tau = 180$ ○: [20] at $Re_\tau = 180$, ◇: [39] at $Re_\theta = 1409$. – –: log-law, $\kappa = 0.38$ and $B = 4.1$. – · –: linear profile and —: mean velocity profile at $Re_\theta = 9700$.

Eq. (8). The accelerating events considered here dominate in number over the decelerating events, and correspond to a forward leaning shear layer structure. Conditional averages for accelerating and decelerating events can be found in, e.g., Fig. 2 in [33].

Alfredsson and Johansson [19] investigated the scaling laws for turbulent channel flow and found that the governing time scale for the near-wall region was a mixture of the inner and outer time scales defined as follows,

$$t_m = \sqrt{t_i t_o}. \tag{13}$$

For further discussion of the interpretation of this timescale, see Alfredsson and Johansson [19]. The frequency of occurrence of the VITA events is shown in Fig. 6 against the averaging time for normalization with the outer, mixed and inner time scales defined as $t_o = \delta_{95}/U_\infty$, $t_m = (t_i t_o)^{0.5}$ and $t_i = \nu/u_\tau^2$, respectively. The choices of definition of the outer and mixed time scales in boundary layer flow are not evident. The most straightforward choice was made here, but an alternative possibility would, e.g., be to use the Clauser–Rotta boundary layer thickness instead of δ_{95} in the expression for the outer timescale t_o. This would however have a negligible influence on the appearance of the collapse in Fig. 6.

The chosen mixed scaling collapses the data also for the boundary layer flow, see Fig. 6, in a satisfactory manner. The important region to look at for collapse is around the peak of the curves. Also for the boundary layer situation the mixed scaling appears significantly better than inner and outer scaling. This result has also been confirmed by Nagano and Houra [40] who argue that the best scaling for the mean bursting period in zero-pressure gradient as well as in adverse pressure gradient boundary layer flows was found with the Taylor time scale ($t_E = \sqrt{2\overline{u^2}/(\partial u/\partial t)^2}$). They also show that the mixed and the Taylor time scales are closely related since the quotient t_E/t_m was found to be constant with Reynolds number.

For very small averaging times one should keep in mind the non-negligible influence of finite probe size for the highest Reynolds numbers. One could argue that a minimum requirement for detecting a shear-layer structure is that the probe size, l^+, should be less than half the width of the shear-layer. As illustrated in Fig. 1 of Johansson et al. [20] the aspect ratio, A, of the

Table 1
Hot-wire experiments used for VITA detection in the buffer layer

	△	∇	∗	+	∘
Re_θ	6700	8200	9700	12600	15200
l^+	6.6	8.2	9.7	12.8	15.8
y^+	14.3	13.8	14.5	14.8	15.2

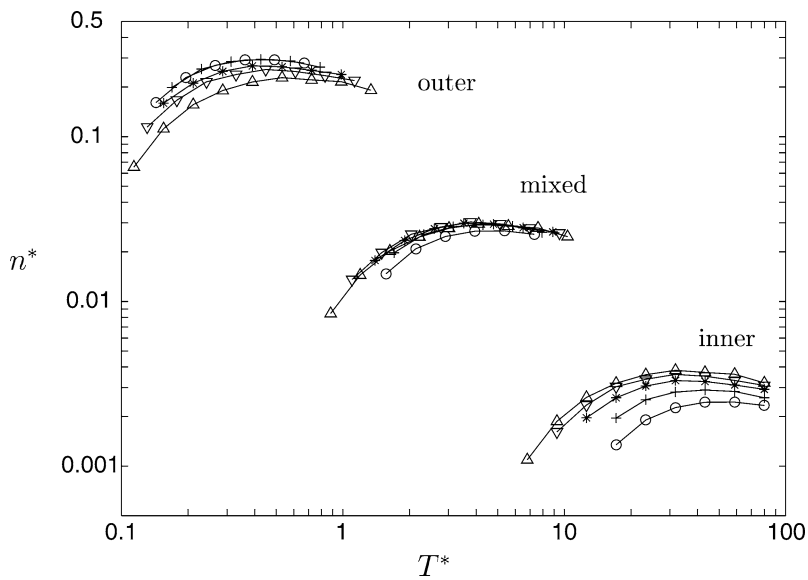

Fig. 6. Frequency of occurrence of VITA events as a function of the averaging time where n^* denotes the frequency normalized with the inverse of t_o, t_m and t_i respectively and T^* the averaging time window normalized with t_o, t_m and t_i respectively. $y^+ = 15$, $k = 1.0$. For symbols see Table 1.

shear-layer structure in the streamwise-spanwise plane at $y^+ = 15$ is about 5–6. Earlier in this paper it was also shown that the propagation velocity, C_p^+ is about 13 at $y^+ = 15$. We can now form a criteria on the minimum averaging time, T^+, as

$$T^+ > \frac{2Al^+}{C_p^+}. \tag{14}$$

The minimum required time averaging window is thus equal to a time based on the probe size which is shown in Table 1 for each Reynolds number used in Fig. 6. At very small time averaging windows, T^+, the number of events is so small that they have a negligible impact on the near-wall dynamics.

In Fig. 6 the outer scaling shows significant spread near the peak, (around $T_o = 0.3$). Outer scaling has been proposed by, e.g., Rao et al. [17], based on the observation that the mean time between bursts multiplied by u_τ^2 was only weakly dependent on the viscosity. They also tried different outer scalings using, (δ^*/U_∞), (δ/U_∞) and (δ/u_τ), where δ^* is the displacement thickness, and found that scaling with the free-stream velocity and the displacement thickness gave the best collapse for Reynolds numbers, Re_θ between 600 and 9000. Antonia and Krogstad [41] found that the scaling of the mean time between ejections or sweeps on a rough surface boundary layer was Reynolds number independent using outer variables for Reynolds numbers, Re_θ between 12000 and 22000. For lower Reynolds numbers they found that the outer scaling was not appropriate. Blackwelder and Haritonidis [18] reported inner scaling for the 'bursting frequency' obtained by the VITA technique. However, their values for the friction velocities (obtained from the near-wall linear profile) deviate substantially from the present correlation for c_f and their mean velocity profiles for different Reynolds numbers show a wide spread in the log-region. This severely affects the conclusions drawn in their study. Our results, in Fig. 6, indicate that inner scaling is not appropriate for the bursting frequency. With the mixed scaling used in Fig. 6 the collapse is good for a large span of Reynolds numbers.

4.4. Wall-shear stress events

The wall shear stress signal is highly intermittent (flatness factor ≈ 4.9) and peaks in the wall-shear stress were used to detect events. In Fig. 7(a) the conditionally averaged wall-shear stress events are shown for different detection threshold levels $k = \{1, 2, 3\}$. Broad peaks are seen that are largely symmetric. Negative events (not considered in this paper) are slightly wider and less pointed as compared to the positive events. Otherwise their shape is similar. The trace of the time signal has the characteristics of a low stable, (with small variation), level for extended periods of time mixed with short intermittent peaks in the wall shear-stress, see Fig. 7(a). In this case detecting on high levels of the time signal itself means that these events are predominantly associated with sweep-like motions of fluid with high velocity from the outer part of the boundary layer that penetrates down to the viscous sublayer. Detection on peaks in the wall-shear stress was used to form conditional averages for the streamwise velocity obtained at a wall-normal separation Δy^+. Conditional averages for the streamwise velocity are shown in Fig. 7(b) for different wall-normal separations above the hot-film used as detector. For increasing wall-distance the conditionally averaged velocity peak is shifted towards negative times indicating a forward leaning structure. In Fig. 8 the data in Fig. 7(b) are re-plotted into lines of constant disturbance velocity (normalized with the local r.m.s.-level) in the (x, y)-plane using the measured propagation velocities (Fig. 5) to transform the time to an x-coordinate. An elongated and forward leaning

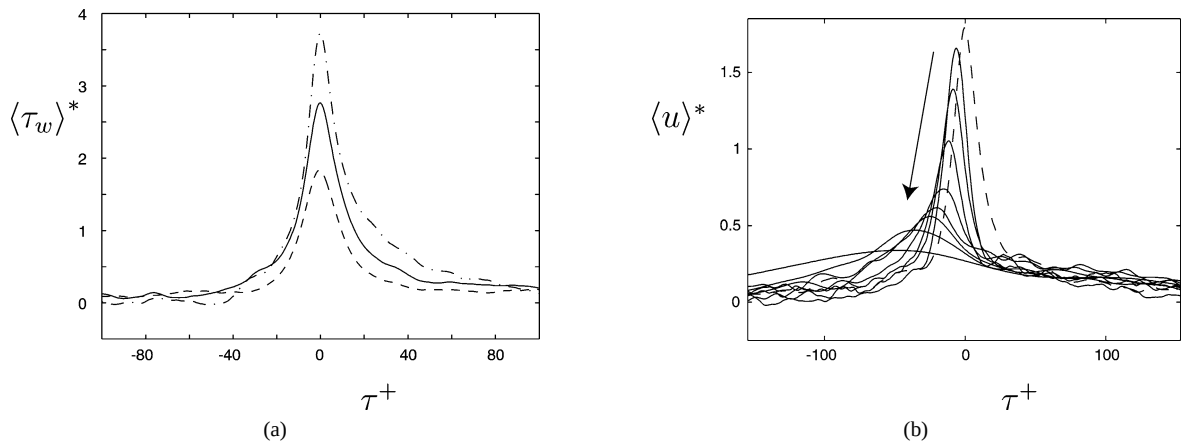

Fig. 7. Detection on positive peaks of τ_w'. $Re_\theta = 9500$. (a) Conditionally averaged wall-shear stress signal normalized with τ_w'. Detection levels, $-\cdot-$: $k = 3$, $-$: $k = 2$, $--$: $k = 1$. (b) Conditionally averaged streamwise velocity, normalized with u′. Detection level $k = 1$. $\Delta x = 0$. $y^+ = \{5.7, 9.6, 16.6, 29.2, 51.7, 92.1, 164, 294\}$. The arrow indicates increasing y^+. $--$: detection signal.

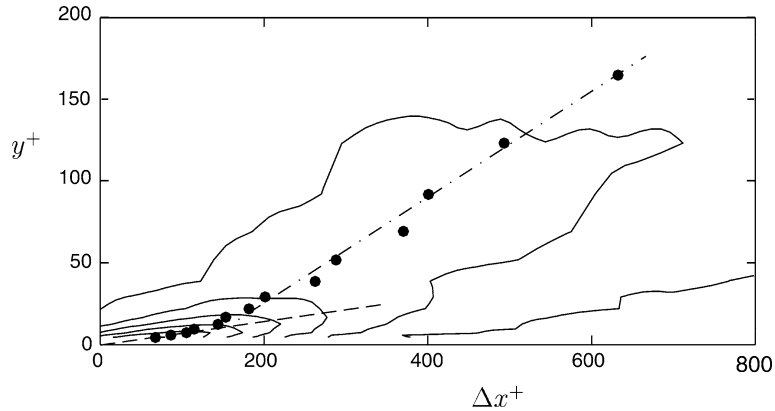

Fig. 8. Conditionally averaged streamwise velocity. Detection of events where $\tau_w > k\tau'_w$. $k = 1$. •: locations of maximum correlation. $-\cdot-$: slope of 18°. $--$: slope of 4°.

high-velocity structure is visible above the high wall-shear event detected at $x = 0$. The peaks of the conditionally averaged velocity in Fig. 7(b) are shown as filled circles and agree well with a shear layer angle above $y^+ = 40$ of about 15° found in many investigations, see, e.g., Johansson et al. [15]. The outermost points are here disregarded because they are very far from the wall. Closest to the wall, i.e., $y^+ < 15$ they reported shear-layer angles of about 7°. In this study it was found to be somewhat smaller (4°). The overall impression from Fig. 8 is that there is a gradual change in the shear angle out to y^+ of about 40 where it becomes constant.

5. Concluding remarks

Near-wall structures in a zero-pressure gradient turbulent boundary layer were studied at high Reynolds numbers. A MEMS-type of hot-film sensor array was used for this purpose together with a hot-wire probe. The small dimension of the hot-film and hot-wire sensors was a necessity for these measurements.

The streak spacing at high Reynolds numbers was studied through filtering of the wall-shear stress signals before constructing the two-point correlation $R_{\tau_w\tau_w}(\Delta z^+)$. While DNS results at low Reynolds number show a distinct negative minimum for separations around $\Delta z^+ = 50$, the correlation (without filtering) for a momentum loss Reynolds number of 9500 indicate a much stronger influence of large scale motions and no real sign of a minimum. By removing contributions from large-scale motions through high-pass filtering, a correlation function similar to that for low Reynolds number flows was recovered, indicating a streak spacing just below 100. It is interesting to note that the optimum cut-off filter frequency corresponds to about 400 viscous units, which is in the range of the typical streak-lengths. At this filter choice close to 90% of the energy (see Fig. 3(b)) is removed before calculation of the correlation, again signifying the influence of large-scale motions for the near-wall dynamics at high Reynolds numbers.

The streak-spacing obtained after filtering, as well as buffer region shear-layer angles and propagation velocities were found to be close to those typically found for low Reynolds number flows.

The frequency of occurrence of shear-layer events and their duration was found to scale with a mixed time scale for a wide range of Reynolds numbers. The mixed scale was taken as the geometric mean of the inner and outer time scales, i.e., the same type of scale as that found by Alfredsson and Johansson [19] to collapse this type of data in turbulent channel flow. One may interpret also this finding as an increasing influence of large scale motions on the near-wall dynamics with increasing Reynolds number.

Acknowledgements

The authors wish to thank Professor Chih-Ming Ho at UCLA for providing us with the MEMS hot-film probe. We would like to thank Professor Henrik Alfredsson for many helpful discussions. We also wish to thank Mr. Ulf Landen and Mr. Marcus Gällstedt who helped with the manufacturing of the experimental set-up. Financial support from NUTEK and The Swedish Research Council is gratefully acknowledged.

References

[1] S.J. Kline, W.C. Reynolds, F.A. Schraub, P.W. Runstadler, The structure of turbulent boundary layers, J. Fluid Mech. 30 (1967) 741–773.
[2] H.T. Kim, S.J. Kline, W.C. Reynolds, The production of turbulence near a smooth wall in a turbulent boundary layer, J. Fluid Mech. 50 (1971) 133–160.

[3] E.R. Corino, R.S. Brodkey, A visual investigation of the wall region turbulent flow, J. Fluid Mech. 37 (1969) 1–30.
[4] C.R. Smith, S.P. Metzler, The characteristics of low-speed streaks in the near-wall region of a turbulent boundary layer, J. Fluid Mech. 129 (1983) 27–54.
[5] L.G. Kovasznay, V. Kibens, R.S. Blackwelder, Large-scale motion in the intermittent region of a turbulent boundary layer, J. Fluid Mech. 41 (1970) 283–325.
[6] Y.M. Yuan, M.R. Mokhtarzadeh-Dehghan, A comparison study of conditional-sampling methods used to detect coherent structures in turbulent boundary layers, Phys. Fluids 6 (6) (1994) 2038–2057.
[7] J.M. Wallace, H. Eckelmann, R. Brodkey, The wall region in turbulent shear flow, J. Fluid Mech. 54 (1972) 39–48.
[8] W.W. Willmarth, S.S. Lu, Structure of the Reynolds stress near the wall, J. Fluid Mech. 55 (1972) 65–92.
[9] R.F. Blackwelder, R.E. Kaplan, On the wall structure of the turbulent boundary layer, J. Fluid Mech. 76 (1976) 89–112.
[10] K.K. Chen, R.F. Blackwelder, Large-scale motion in a turbulent boundary layer, J. Fluid Mech. 89 (1978) 1–31.
[11] S. Tardu, Characteristics of single and clusters of bursting events in the inner layer. Part 1: VITA events, Exp. Fluids 20 (2) 112–124.
[12] H.-P. Kreplin, H. Eckelmann, Propagation of pertubations in the viscous sublayer and adjacent wall region, J. Fluid Mech. 95 (1979) 305–322.
[13] M.R. Head, P. Bandyopadhyay, New aspects of turbulent boundary layer structure, J. Fluid Mech. 107 (1981) 297–338.
[14] A.K. Gupta, J. Laufer, R.E. Kaplan, Spatial structure in the viscous sublayer, J. Fluid Mech. 50 (1971) 493–512.
[15] A.V. Johansson, P.H. Alfredsson, H. Eckelmann, On the evolution of shear layer structures in near wall turbulence, in: G. Compte-Bellot, J. Mathieu (Eds.), Advances in Turbulence, Springer-Verlag, 1987, pp. 383–390.
[16] C.E. Wark, H.M. Nagib, Experimental investigation of coherent structures in turbulent boundary layers, J. Fluid Mech. 230 (1991) 183–208.
[17] K.N. Rao, R. Narasima, M. Badri Narayanan, The “bursting” phenomenon in a turbulent boundary layer, J. Fluid Mech. 48 (1971) 339–352.
[18] R.F. Blackwelder, J.H. Haritonidis, The bursting frequency in turbulent boundary layers, J. Fluid Mech. 132 (1983) 87–103.
[19] P.H. Alfredsson, A.V. Johansson, Time scales in turbulent channel flow, Phys. Fluids A 27 (8) (1984) 1974–1981.
[20] A.V. Johansson, P.H. Alfredsson, J. Kim, Evolution and dynamics of shear-layer structures in near-wall turbulence, J. Fluid Mech. 224 (1991) 579–599.
[21] S.K. Robinson, Coherent motions in the turbulent boundary layer, Ann. Rev. Fluid Mech. 23 (1991) 601–639.
[22] A.K.M.F. Hussain, Coherent structures and turbulence, J. Fluid Mech. 173 (1986) 303–356.
[23] H.E. Fiedler, Coherent structures, in: Advances in Turbulence, Vol. 32, Springer-Verlag, Berlin, 1986, pp. 320–336.
[24] A.V. Johansson, A low speed wind-tunnel with extreme flow quality – design and tests, in: Prog. ICAS Congress 1992, ICAS-92-3.8.1, 1992, pp. 1603–1611.
[25] F. Jiang, Y.-C. Tai, B. Gupta, R. Goodman, S. Tung, J.B. Huang, C.-M. Ho, A surface-micromachined shear stress imager, in: 1996 IEEE Micro Electro Mechanical Systems Workshop (MEMS ’96), 1996, pp. 110–115.
[26] F. Jiang, Y.-C. Tai, K. Walsh, T. Tsao, G.B. Lee, C.-H. Ho, A flexible mems technology and its first application to shear stress sensor skin, in: 1997 IEEE Micro Electro Mechanical Systems Workshop (MEMS ’97), 1997, pp. 465–470.
[27] C.-M. Ho, Y.-C. Tai, Micro-electro-mechanical-systems (MEMS) and fluid flows, Ann. Rev. Fluid Mech. 30 (1998) 579–612.
[28] H.H. Fernholz, G. Janke, M. Schober, P.M. Wagner, D. Warnack, New developments and applications of skin-friction measuring techniques, Meas. Sci. Technol. 7 (1996) 1396–1409.
[29] J.M. Österlund, A.V. Johansson, H.M. Nagib, M.H. Hites, A note on the overlap region in turbulent boundary layers, Phys. Fluids 12 (1) (2000) 1–4.
[30] J.M.Österlund, Experimental studies of zero pressure-gradient turbulent boundary-layer flow, Ph.D. thesis, Department of Mechanics, Royal Institute of Technology, Stockholm, 1999.
[31] H.H. Fernholz, P.J. Finley, The incompressible zero-pressure-gradient turbulent boundary layer: An assessment of the data, Prog. Aerospace Sci. 32 (1996) 245–311.
[32] A.E. Perry, S. Hafez, M.S. Chong, A possible reinterpretation of the Princeton superpipe data, J. Fluid Mech. 439 (2001) 395–401.
[33] A.V. Johansson, P.H. Alfredsson, On the structure of turbulent channel flow, J. Fluid Mech. 122 (1982) 295–314.
[34] A.V. Johansson, J.-Y. Her, J.H. Haritonidis, On the generation of high-amplitude wall-pressure peaks in turbulent boundary layers and spots, J. Fluid Mech. 175 (1987) 119–142.
[35] J. Kim, P. Moin, R. Moser, Turbulence statistics in fully developed channel flow, J. Fluid Mech. 177 (1987) 133–166.
[36] R.D. Moser, J. Kim, N.N. Mansour, Direct numerical simulation of turbulent channel flow up to $Re_\theta = 590$, Phys. Fluids 11 (4) (1999) 943–945.
[37] A.M. Naguib, C.E. Wark, An investigation of wall-layer dynamics using a combined temporal filtering and correlation technique, J. Fluid Mech. 243 (1992) 541–560.
[38] H. Abe, H. Kawamura, A study of turbulence thermal structure in a channel flow through DNS up to $Re_\tau = 640$ with $Pr = 0.025$ and 0.71, in: Advances in Turbulence IX, Cimne, Barcelona, 2002, pp. 399–402.
[39] P.-Å. Krogstad, J.H. Kaspersen, S. Rimestad, Convection velocities in a turbulent boundary layer, Phys. Fluids 10 (4) (1998) 949–957.
[40] Y. Nagano, T. Houra, Scaling of near-wall structures in turbulent boundary layers subjected to adverse pressure gradient, in: IUTAM Symposium on Reynolds Number Scaling in Turbulent Flow, Princeton University Press, Princeton, NJ, 2002, pp. 541–560.
[41] R.A. Antonia, P.-Å. Krogstad, Scaling of the bursting period in turbulent rough wall boundary layers, Exp. Fluids 15 (1) (1993) 82–84.